Effect of Dispersed Intermetallic Particles on Microstructural Evolution in the Friction Stir Weld of a Fine-Grained Magnesium Alloy

JINSUN LIAO, NAOTSUGU YAMAMOTO, and KAZUHIRO NAKATA

A fine-grained Mg alloy with copious dispersed Al_6Mn particles was friction stir (FS) welded, and microstructures at the stir zones (SZs) were investigated intensively and compared to those in a coarse-grained Mg alloy, which had identical chemical compositions with the fine-grained one but much less Al_6Mn particles. It is found that the grain size at the SZs is a little coarser than that of the base material in the fine-grained alloy, while it becomes much finer in the coarse-grained one. Under the same welding conditions, however, the grain size at the SZs in the fine-grained alloy is much smaller than that in the coarse-grained one. These experimental results are explained in terms of a grain growth mechanism proposed in the present study. Transmission electron microscopy (TEM) examination shows that the dispersed Al_6Mn particles can suppress grain growth *via* Zener pinning, and consequently result in smaller grains at the SZs in the fine-grained alloy.

DOI: 10.1007/s11661-009-9921-2

I. INTRODUCTION

WITH the increase in the need to reduce fuel consumption and thus carbon dioxide emission, lightweighting of vehicles is becoming more and more urgent for automotive industries.[1] Magnesium alloy, the lightest structural metal, is a promising material for reducing the weight of automobiles; however, its automotive application is limited to a single-component level mainly due to its low strength and poor formability.[2] It is therefore important to improve the strength of magnesium alloys in order to broaden their application in the automotive field as well as other industries.

Grain refinement is an effective method to increase the strength of metals. Some severe plastic deformation processes, such as equal-channel angular pressing (ECAP),[3,4] accumulative roll bonding (ARB),[5–7] and the roll compaction process (RCP),[8,9] have been developed and applied to steels, aluminum alloys, and magnesium alloys to refine their grain sizes. By employing the roll compaction process, bulky magnesium alloys with fine-grained microstructures have been manufactured, and their strengths have been remarkably increased.[9]

In order to apply magnesium alloys to structures, on the other hand, welding or joining technology is indispensable. Friction stir (FS) welding, a solid-state joining process, has attracted great interest from scientists and engineers, and FS welding of aluminum and magnesium alloys has been intensively investigated.[10–24] It has been demonstrated that very fine grains of 1 to 10 μm are created in the center of FS welds, because of the extraordinary level of plastic deformation or strain rate induced by a rotating tool, reaching an effective strain in excess of 40.[25] The fine-grained microstructures in FS welds are formed due to dynamic recrystallization[12,25] and can be generally interpreted using the Zener–Hollomon parameter.[25–27] Recently, a continuous recrystallization mechanism has been proposed to explain the recrystallized fine-grained microstructures in FS welds.[11,28] Since the structures in FS welds are usually finer than those of base materials for most commercial metals or alloys, the mechanical performance in FS welds is enhanced in many cases. Indeed, FS processing, a new surface modification technology evolved from FS welding, has been developed to improve mechanical properties on the surface of metals.[29]

Concerning the factors controlling microstructures in FS welds, it has been shown that the grain size in FS welds of aluminum alloys is principally decided by welding parameters, and the effect of original grain structures can be ignored.[30–32] A recent study on AZ31 magnesium alloy has also proven that the initial grain size has little influence on the recrystallized grain structures in the case of high effective strain, which are mainly dependent on the Zener–Hollomon parameter.[33] However, the effects of intermetallic phases have not been addressed in the previous studies.

The formation of fine-grained microstructures in the welds, as mentioned previously, makes FS welding an ideal candidate for joining fine-grained alloys. There are several studies on FS welding of extra-fine-grained aluminum alloys,[31,32] but no reports on FS welding of

JINSUN LIAO, Senior Research Engineer and Manager, and NAOTSUGU YAMAMOTO, Research Engineer, are with Technology Development Headquarters, Kurimoto Ltd., Osaka 559-0021, Japan. Contact e-mail: j_liao@kurimoto.co.jp KAZUHIRO NAKATA, Professor, is with the Joining and Welding Research Institute, Osaka University, Osaka 567-0047, Japan.

Manuscript submitted February 13, 2009.
Article published online July 28, 2009

fine-grained magnesium alloys. In the present work, the FS weldability of a fine-grained AZ31B with copious dispersed Al_6Mn particles was investigated, and the microstructures in FS welds were studied intensively. The effect of the dispersed intermetallic Al_6Mn particles on microstructural evolution in FS welds was discussed.

II. EXPERIMENTAL DETAILS

The fine-grained AZ31B employed in the present research was produced *via* the RCP, a severe plastic deformation process. Details of the RCP were described in References 8 and 9. An AZ31B ingot (Mg-2.96Al-1.00Zn-0.36Mn, mass pct) was used as the starting material for grain refinement. Powders chipped from the AZ31B ingot were severely compressed by the RCP at room temperature. The severe plastic deformation processed powders were collected and consolidated to billets and then hot extruded to a plate of 75 mm in width and 4 mm in thickness.

The roll compaction processed fine-grained AZ31B plates of 250 mm in length were butt-welded together along the extrusion direction using FS welding equipment, as illustrated in Figure 1. The rotating tool for FS welding, which was made from tool steel, consisted of a concave shoulder of 15 mm in diameter and a pin with right-hand threads of 3.9 mm in length and 5 mm in diameter. The rotation speed was kept constant at 1250 rpm, and the traverse speed (*i.e.*, welding speed) was varied from 250 to 750 mm/min. During FS welding, the temperature was measured at "a," "b," and "c" points, which were 1.5, 2.5, and 3.5 mm away from the tool center, and at the location of the stir zone (SZ), the thermomechanically affected zone (TMAZ), and the heat-affected zone (HAZ), respectively. In the present work, the advancing side was marked "AS" and the retreating side "RS." In addition, coarse-grained AZ31B plates, which were produced directly from the AZ31B ingot *via* conventional hot extrusion (denoted as CHE AZ31B, in the present work) and had identical chemical compositions and dimensions with the roll compaction processed AZ31B plates, were also butt-welded under the same welding conditions, for a comparison.

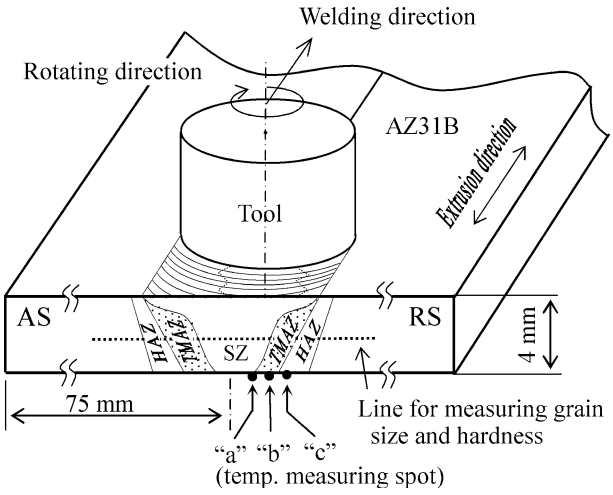

Fig. 1—Schematic illustration of FS welding.

After FS welding, the Vickers hardness profiles of the welds were measured on cross sections perpendicular to the welding direction, and microstructures in the welds were characterized by means of optical microscopy and transmission electron microscopy (TEM). Specimens for optical microscopy were polished and then etched with a solution of 10 g picric acid, 175 mL ethanol, 25 mL acetic acid, and 25 mL distilled water. Thin foils for TEM were prepared by using a focused ion beam instrument or an ion slicer and examined with a transmission electron microscope (JEOL* 2010) operated at 160 to 200 kV. Chemical compositions of intermetallic particles were analyzed with an energy dispersive X-ray (EDX) spectrometer equipped to the transmission electron microscope.

*JEOL is a trademark of Japan Electron Optics Ltd., Tokyo.

III. RESULTS AND DISCUSSION

A. *Microstructure of Roll Compaction Processed AZ31B*

Microstructures of roll compaction processed AZ31B and CHE AZ31B are shown in Figure 2. The roll

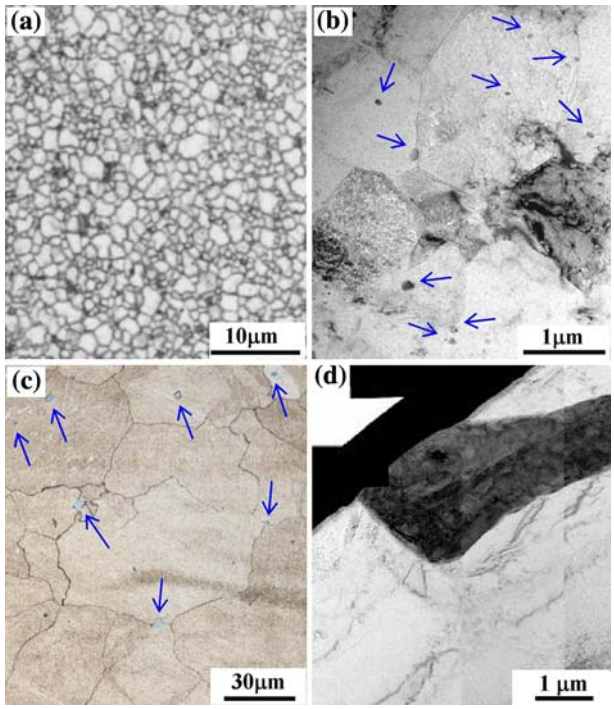

Fig. 2—Microstructures of roll compaction processed AZ31B and CHE AZ31B: (*a*) and (*b*) optical microstructure and TEM image of intermetallic particles in roll compaction processed AZ31B, respectively; and (*c*) and (*d*) optical microstructure and TEM image of an intermetallic particle in CHE AZ31B, respectively.

compaction processed AZ31B exhibits essentially equiaxed fine grains of approximately 0.6 to 3 μm (Figures 2(a) and (b)), and its average grain size is 1.9 μm. The boundaries of the severe plastic deformation processed powders are hardly observed with optical microscopy and TEM, indicating that most of the power boundaries have disappeared after hot extrusion, probably because friction and dynamic recrystallization occurred at the boundaries of powders during hot extrusion. There are a lot of particles from several tens of nanometers to about 200 nm in the interior of grains and at grain boundaries of the roll compaction processed AZ31B (Figure 2(b)). Comparatively, the grains in the CHE AZ31B are much coarser (Figure 2(c)), and its average grain is 44 μ. Some particles are also observed in the CHE AZ31B (Figures 2(c) and (d)), but the size of the particles is much larger (several microns), and the number of them much less, as compared to those in the roll compaction processed AZ31B. These particles are Al_6Mn (orthorhombic, $a = 0.75551$, $b = 0.64994$, and $c = 0.88724$ nm) in both the roll compaction processed AZ31B and CHE AZ31B, as shown in Figure 3, where the TEM image, electron diffraction pattern, and EDX analysis result of a particle in the roll compaction processed AZ31B are presented as an example.

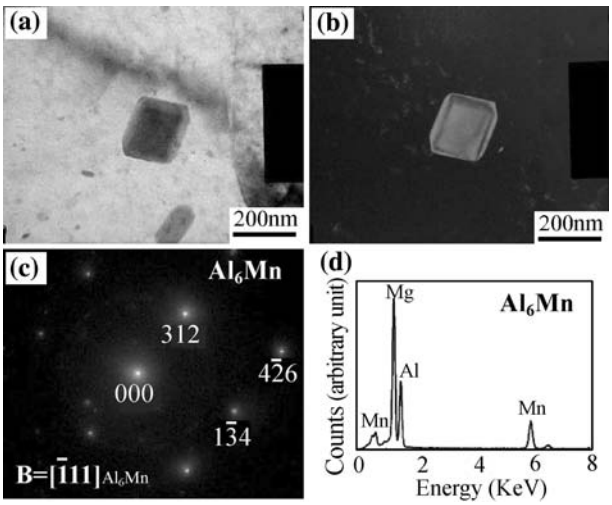

Fig. 3—Intermetallic particle in roll compaction processed AZ31B: (*a*) and (*b*) TEM image of an intermetallic particle and its dark field, (*c*) electron diffraction pattern of the intermetallic particle, and (*d*) EDX analysis result of the intermetallic particle.

Neither $Mg_{17}Al_{12}$ phase nor oxide particles are observed in both the roll compaction processed and CHE AZ31B. It should be noted that many $Mg_{17}Al_{12}$ and a few Al_6Mn particles exist in the AZ31B ingot, and the size of these intermetallic particles is several microns, on the same level as those in the CHE AZ31B. Microstructural comparison among the roll compaction processed AZ31B, CHE AZ31B, and AZ31B ingot indicates that Al_6Mn particles in the AZ31B ingot are refined and dispersed by the RCP, but not by hot extrusion. The $Mg_{17}Al_{12}$ phase in the AZ31B ingot has been decomposed after hot extrusion.

B. *FS Weldability of Roll Compaction Processed AZ31B*

Figure 4 reveals surface appearances and cross sections of FS welded joints of roll compaction processed AZ31B at various welding speeds. There is almost no difference in the shape of the SZs in these FS welds. Sound FS welded joints without any defects are

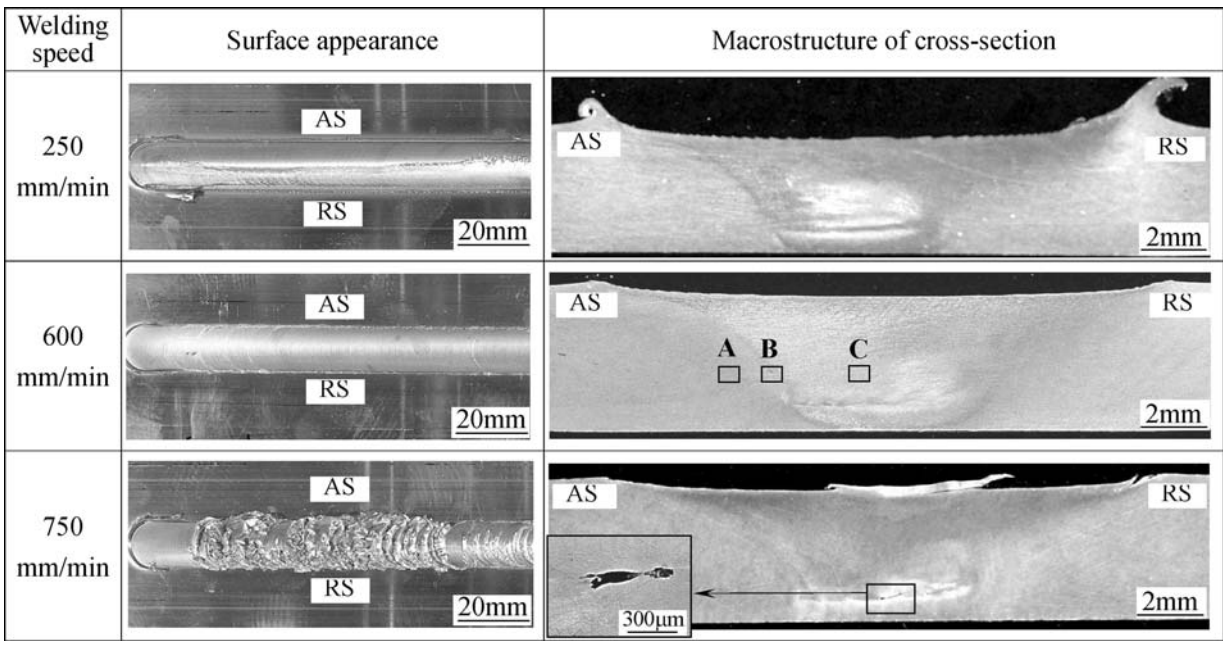

Fig. 4—Surface appearances and cross-sectional macrostructures of FS welded joints of roll compaction processed AZ31B at various welding speeds.

obtained at welding speeds of 250 to 600 mm/min, a considerably wide range. When the welding speed is increased to 750 mm/min, however, the surface of the FS weld becomes rough, and a small cavity-like defect forms at the lower part of the weld, because heat input per unit length of the weld is insufficient and thus extensive plastic flow cannot be achieved in the weld. It is important to note that the CHE AZ31B is also successfully FS welded without any defect at welding speeds of 250 to 600 mm/min.

C. *Microstructures in FS Welds*

Figure 5 gives microstructures at regions marked "A," "B," and "C" in Figure 4, which correspond to the HAZ, TMAZ, and SZ in the FS weld of the roll compaction processed AZ31B at a welding speed of 600 mm/min, respectively. Grain structures at the HAZ (Figure 5(a)) and SZ (Figure 5(c)) are equiaxed, similar to that of the base material (Figure 2(a)), while TMAZ exhibits an extended grain structure (Figure 5(b)). It can be seen that the grain sizes in these regions become a little larger compared to that of the base material. Transmission electron microscopy reveals that there are many dispersed Al_6Mn particles not only in the interior of grains and but also at grain boundaries (shown by arrows in Figures 5(d) and (e)), and some of the dispersed Al_6Mn particles at grain boundaries seem to play a role in inhibiting the motion of grain boundaries *via* Zener pinning, which will be discussed in Section III–E. From the microstructural observations at the TMAZ and SZ, it is conceivable that continuous recrystallization has occurred at the SZ and at TMAZ in part.

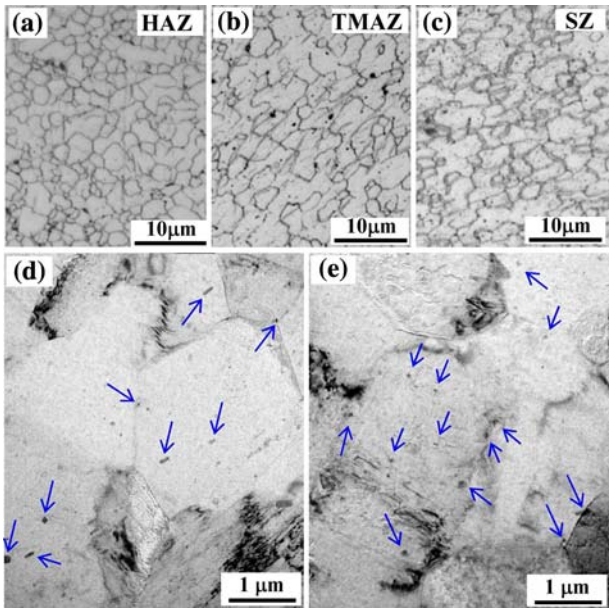

Fig. 5—Microstructures in the FS weld of roll compaction processed AZ31B at a welding speed of 600 mm/min: (*a*) through (*c*) optical microstructures at the HAZ, TMAZ, and SZ, respectively; and (*d*) and (*e*) TEM images of microstructures and Al_6Mn particles at the TMAZ and SZ, respectively.

The microstructure at the SZ of CHE AZ31B at a welding speed of 600 mm/min is presented in Figure 6. Unlike roll compaction processed AZ31B, the microstructure at the SZ of the CHE AZ31B becomes much finer than that of the base material (Figure 2(c)). Optical microscopy and TEM show that the size of Al_6Mn particles at the SZ is larger, and the number is few, like those in the base material. Most of these Al_6Mn particles are observed in the interior of grains.

Figure 7 shows grain size profiles at the midthickness across the welds of both roll compaction processed AZ31B and CHE AZ31B at a welding speed of 600 mm/min. For the roll compaction processed AZ31B, grain sizes in the FS weld and base material are on the same level. The average grain size at the SZ is 2.4 μm, slightly larger than that of the base material, 1.9 μm. In contrast, the grain size at the SZ of the CHE AZ31B is remarkably decreased as compared to that of

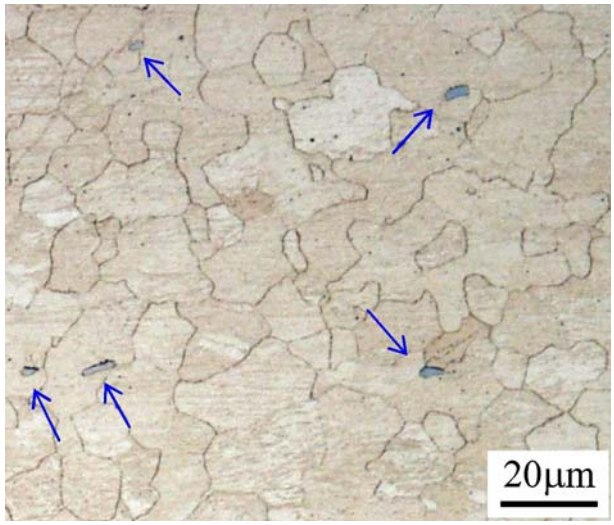

Fig. 6—Microstructure at the SZ of CHE AZ31B at a welding speed of 600 mm/min.

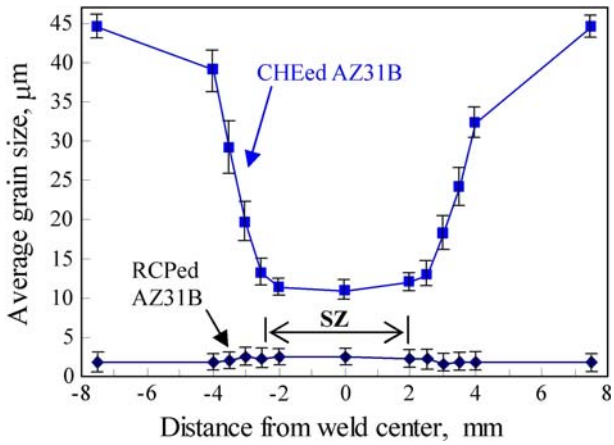

Fig. 7—Variation of grain size across FS-welded joints of roll compaction processed AZ31B and CHE AZ31B at a welding speed of 600 mm/min.

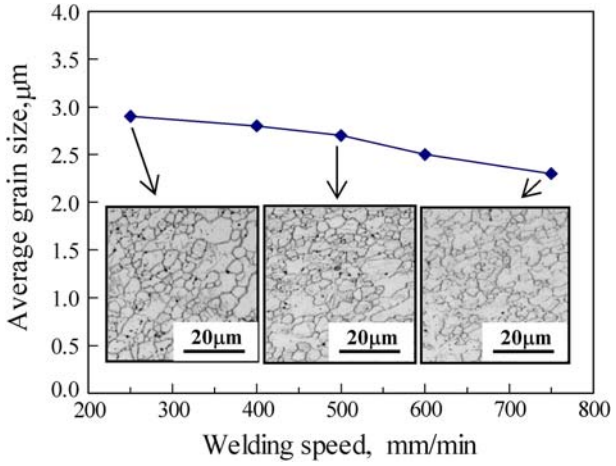

Fig. 8—Effect of welding speed on grain size at the SZs of roll compaction processed AZ31B.

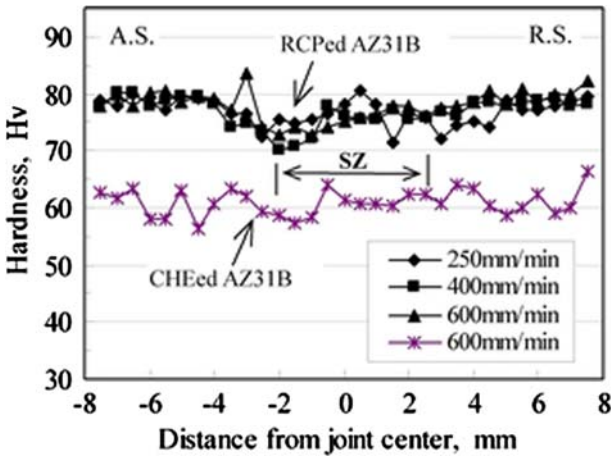

Fig. 9—Hardness across the cross section of FS-welded joints of roll compaction processed AZ31B and CHE AZ31B.

the base material. Although welding parameters as well as chemical compositions and specimen dimensions, by which the grain size at the SZs is almost determined as mentioned earlier,[30–32] are the same for the two magnesium alloys, the grain size is much smaller at the SZ of the roll compaction processed AZ31B than the CHE AZ31B. Hence, it is believed that the difference in grain size at the SZs of the two magnesium alloys is mainly due to the dispersed Al_6Mn particles. However, it has been demonstrated that the grain size of magnesium alloys may have an influence on the deformation behavior and, consequently, the thermal history in the FS welds especially when the average grain size is less than 3 μm;[34,35] therefore, it is more reasonable to think that the dispersed Al_6Mn particle is an important but not sole factor responsible for the fine-grained microstructures in FS welds of the roll compaction processed AZ31B.

Figure 8 illustrates the effect of welding speed on grain size at the center of the SZs of roll compaction processed AZ31B. With an increase in welding speed, grain size at the center of the SZ slightly decreases, due to less welding heat input per unit length of welded joint, which means lower peak temperature and shorter heating time for recrystallization and subsequent grain growth. As compared to the results of previous research,[21,22,24] however, the grain size variant with welding speed is not remarkable at the SZs of roll compaction processed AZ31B, indicating that grain growth at the SZs of roll compaction processed AZ31B is probably inhibited by the dispersed Al_6Mn particles.

D. *Hardness in FS Welds*

Figure 9 gives microhardness profiles at midthickness across welds of roll compaction processed AZ31B at welding speeds of 250, 400, and 600 mm/min, in comparison with that of CHE AZ31B at welding speed of 600 mm/min. For all welds of the roll compaction processed AZ31B at welding speeds from 250 to 600 mm/min, although there is a slight hardness drop of approximately 5 to 8 HV at the advancing side of the SZ, the major part of FS welds retains roughly the hardness of the base material, implying that FS welding may prevent obvious deterioration in mechanical properties of the welded joint for roll compaction processed AZ31B. It can also be seen that the hardness in the FS welds of roll compaction processed AZ31B is little affected by welding speed. For the CHE AZ31B welded at 600 mm/min, there is no apparent change in the hardness between the FS weld and base material, although the average hardness of the FS weld is slightly higher than that of the base material. This is consistent with previous studies,[23,36] which have reported that there is only a weak influence of grain size on hardness in the FS welds of magnesium alloys.[23,37] It should be noted that the hardness in the FS welds of roll compaction processed AZ31B is much higher than that in the FS weld of CHE AZ31B, probably due to both the strengthening effect of dispersed Al_6Mn particles and the grain size effect.

E. *Effect of Intermetallic Particles on Microstructural Evolution in FS Welds*

It is well known that recrystallization occurs at the SZs during FS welding of aluminum alloys and magnesium alloys.[10–24] The recrystallization also takes place at the SZs of both roll compaction processed AZ31B and CHE AZ31B alloys. Until now, mainly two kinds of mechanisms have been proposed to explain the recrystallized structures in FS welds. Rhodes *et al.*[12] suggest that the recrystallization in FS welds is the conventional dynamic recrystallization;[38] *i.e.*, the nucleation of high-angle grain boundaries concurrent with the deformation induced by stirring and the growth of new grains are included in the recrystallization. On the other hand, Su *et al.*[11] and Jata *et al.*[28] propose that continuous recrystallization,[38] which is characterized by a strain-induced progressive rotation of subgrains with little boundary migration, is the primary mechanism during FS welding. It is assumed that four stages are included

in the continuous recrystallization process: (1) dislocation introduction; (2) formation of low-angle boundary subgrains by dynamic recovery; (3) formation of the equiaxed recrystallized grains with high-angle boundaries, which results from growth and rotation of small subgrains due to continuous introduction and accommodating of dislocations; and (4) repeated introduction of dislocations and partial recovery of recrystallized grains. These mechanisms focus on the phenomenon that grain size becomes smaller at the SZs than base material, but cannot explain the grain-coarsening phenomenon in FS welds, which has been observed in the present work as well as some previous studies.[17,31,32] The grain-coarsening phenomenon must be rationalized in order to comprehensively understand the microstructure evolution in FS welds.

To explain the grain-coarsening phenomenon in FS welds, the present authors suggest that grain growth is an important step during the structural evolution in FS welds, regardless of whether the new grains were formed by dynamic recrystallization or a continuous recrystallization reaction. That is to say, the grain structures in FS welds should experience two steps: the formation of new grains *via* recrystallization and grain growth of the recrystallized new grains.

Assuming that the recrystallized grains grow statically under ideal conditions, the grain growth kinetics can be expressed by

$$D^2 - D_0^2 = A \exp(-Q/RT)t \quad [1]$$

where D_0 is the initially created grain size, D the final grain size, Q the activation energy for grain growth, R the ideal gas constant, T the absolute temperature, t the time, and A is a constant. Since the initially created grain size is 25 to 100 nm,[12] much smaller than the final grain size in FS welds, the D_0^2 value can be ignored. Hence, Eq. [1] is written as

$$D^2 = A \exp(-Q/RT)t \quad [2]$$

Considering that the temperature changes continuously with time during FS welding, it is more reasonable that

$$D^2 = A \int_{t_0}^{t_1} \exp(-Q/RT)dt \quad [3]$$

where t_0 is the time when recrystallization ends and grain growth begins, and t_1 is the time when grain growth completes. From Eq. [3], it is easily understood that grain size is determined by the activation energy for grain growth Q and thermal histories, which are expressed as T and t.

For a given alloy, the activation energy for grain growth Q is almost unchangeable, so that grain size is principally dependent on the thermal histories during FS welding, which is mainly dependent on welding conditions and specimen dimension. That is to say, if the same welding conditions and specimen dimensions are chosen for a given alloy, the grain size at the SZs is almost identical, and this has been proved by some previous research.[31,32] Because of this, it can be believed that finer grains at the SZs of the roll compaction processed AZ31B are, at least partly, attributed to the presence of the dispersed Al_6Mn particles in the roll compaction processed AZ31B in the present study. In fact, it has been demonstrated that the presence of dispersed intermetallic particles can increase the activation energy for grain growth,[39] which is probably the reason that the grain size at the SZs becomes smaller in the roll compaction processed AZ31B, as can be understood from Eq. [3]. Transmission electron microscopy examination reveals that grain boundary migration at the SZs of the roll compaction processed AZ 31B is inhibited *via* Zener pinning of Al_6Mn particles, as shown in Figure 10.

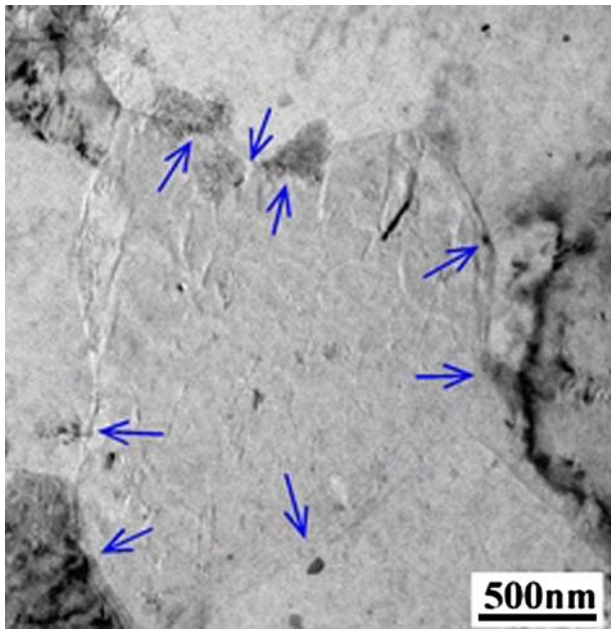

Fig. 10—TEM image of Al_6Mn particles at grain boundaries at the SZ of roll compaction processed AZ31B (welding speed: 600 mm/min), showing Zener pinning of Al_6Mn particles.

For most Mg-Al-Zn magnesium alloys, $Mg_{17}Al_{12}$ is a common intermetallic phase at room temperature. However, this intermetallic phase decomposes and dissolves into the matrix at temperatures above approximately 500 to 630 K, depending on Al content, as illustrated by the Mg-Al binary phase diagram.[40] Actually, temperature measurement indicates that the peak temperature experienced in the FS welds of CHE AZ31B is much higher than 630 K during FS welding, as shown in Figure 11. In the cooling period during FS welding, the precipitation of the $Mg_{17}Al_{12}$ phase is depressed due to the high cooling rate. This is why the $Mg_{17}Al_{12}$ phase is not observed in the FS welds of magnesium alloys.[18,19,36,41] Because of this, the $Mg_{17}Al_{12}$ phase in the magnesium alloy has little influence on the microstructural evolution at the SZs of FS welds.

In contrast to the $Mg_{17}Al_{12}$ phase, Al_6Mn particles are capable of suppressing grain growth in the FS welds *via* inhibition of grain boundary migration, as mentioned previously. Since the decomposition temperature

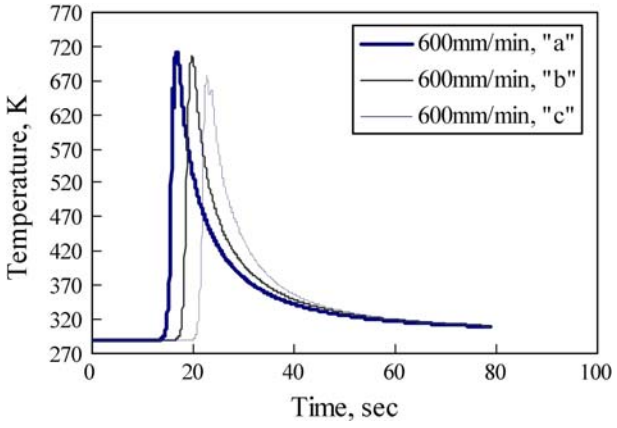

Fig. 11—Thermal histories at various locations in the FS weld of CHE AZ31B during FS welding (welding speed: 600 mm/min).

of Al_6Mn is about 931 K, according to the Al-Mn binary phase diagram,[40] much higher than the peak temperature experienced during FS welding of magnesium alloys, Al_6Mn particles can remain in the FS welds and suppress grain growth *via* Zener pinning.

In order to obtain the Zener pinning effect, tiny and dispersed intermetallic particles are necessary.[42] The RCP provides an effective method for the refinement and dispersion of intermetallic particles. Besides, other severe plastic deformation processes, such as ECAP and ARB, can also refine and disperse intermetallic particles.[3–7]

From the preceding discussion, it can be concluded that dispersed intermetallic particles with high decomposition temperature are beneficial to suppressing grain growth and, consequently, the formation of fine-grained microstructures in FS welds. The addition of intermetallic phase forming elements such as Mn, Ca, and rare earth elements to magnesium alloys, together with the application of a severe plastic deformation process, by which tiny intermetallic particles with high decomposition temperatures are produced and dispersed in magnesium alloys, is helpful to manufacturing fine-grained magnesium alloys and obtaining fine-grained microstructures in their FS welds.

IV. CONCLUSIONS

A fine-grained AZ31B with copious dispersed Al_6Mn particles produced by a severe plastic deformation process was FS welded, and the microstructures in the FS welds were intensively examined by means of optical microscopy and TEM, and compared with those of a conventionally hot-extruded AZ31B with comparatively coarse grains and identical chemical compositions but much less Al_6Mn particles. The effect of dispersed Al_6Mn particles on microstructural evolution at the SZs was discussed. The results can be summarized as follows.

1. The roll compaction processed fine-grained AZ31B magnesium alloy is successfully butt-welded without any defect in welds at welding speeds of 250 to 600 mm/min, when the rotation speed of the tool is kept constant at 1250 rpm. All FS welds have fine-grained microstructures and high hardness, on the same level as the base material, implying that FS welding may prevent obvious deterioration in mechanical properties of welded joints for the roll compaction processed fine-grained magnesium alloy.
2. The grain size at the SZs is a little larger than that of the base material in roll compaction processed AZ31B, whereas it becomes much smaller in CHE AZ31B. Under the same welding conditions, the grain size is much smaller at the SZs of roll compaction processed AZ31B than CHE AZ31B. These results can be explained according to the grain growth mechanism proposed in the present study.
3. The grain structure at the SZs, experiencing recrystallization and subsequent grain growth, is principally determined by the grain growth process, in which the welding-induced thermal histories and the activation energy for grain growth are two important factors. The dispersed Al_6Mn particles suppress grain growth *via* Zener pinning and, consequently, result in finer grains at the SZs in the roll compaction processed fine-grained AZ31B.

REFERENCES

1. J.A. Carpenter, J. Jackman, N. Li, R.J. Osborme, B.R. Powell, and P. Sklad: *Mater. Sci. Forum*, 2007, vols. 546–549, pp. 11–24.
2. A.A. Luo, E.A. Nyberg, K. Sadayappan, and W. Shi: *Magnes. Technol.,* 2008, pp. 3–10.
3. Y. Iwahashi, J.T. Wang, Z. Hirota, and T.G. Langdon: *Scripta Mater.*, 1996, vol. 35, pp. 143–46.
4. K. Nakashima, Z. Hirota, M. Nemoto, and T.G. Langdon: *Acta Mater.*, 1998, vol. 46, pp. 1589–99.
5. S. Saito, H. Utsunomiya, N. Tsuji, and T. Sakai: *Acta Mater.*, 1999, vol. 47, pp. 579–83.
6. N. Tsuji, Y. Saito, S.H. Lee, and Y. Minamino: *Adv. Eng. Mater.*, 2003, vol. 5, pp. 338–34.
7. H. Fujii, R. Ueji, R. Cui, K. Nakata, and K. Nogi: *Trans. JWRI*, 2006, vol. 35, pp. 47–52.
8. K. Kondoh: *Magnes. Technol.,* 2005 pp. 77–80.
9. K. Kaneko, S. Shiozaki, K. Kondoh, H. Oginuma, and T. Akita: *Mater. Jpn.*, 2006, vol. 45, pp. 54–56.
10. K.V. Jata, K.K. Sankaran, and J.J. Rushau: *Metall. Mater. Trans. A*, 2000, vol. 31A, pp. 2181–92.
11. J.-Q Su, T.W. Nelson, R. Mishra, and M.W. Mahoney: *Acta Mater.*, 2003, vol. 51, pp. 713–29.
12. G.G. Rhodes, M.W. Mahoney, W.H. Bingel, and M. Calabrese: *Scripta Mater.*, 2003, vol. 48, pp. 1451–55.
13. C.J. Dawes and M.W. Thomas: *Weld. J.*, 1996, vol. 75, pp. 41–45.
14. C.J. Dawes: *Proc. 6th Int. Symp. of JWS*, JWS, Nagoya, Japan, 1996, pp. 711–18.
15. Y.S. Sato, S.H.C. Park, and H. Kokawa: *Metall. Mater. Trans. A*, 2001, vol. 32A, pp. 3033–42.
16. T.U. Seidel and A.P. Reynolds: *Metall. Mater. Trans. A*, 2001, vol. 32A, pp. 2879–84.
17. W.B. Lee, Y.M. Yeon, and S.B. Jung: *Mater. Sci. Technol.*, 2003, vol. 19, pp. 785–90.
18. S.C. Park, Y.S. Sato, and H. Kokawa: *Metall. Mater. Trans. A*, 2003, vol. 34A, pp. 987–94.
19. S.H.C. Park, Y.S. Sato, and H. Kokawa: *J. Mater. Sci.*, 2003, vol. 38, pp. 4379–83.
20. S.H.C. Park, Y.S. Sato, and H. Kokawa: *Scripta Mater.*, 2003, vol. 49, pp. 161–66.
21. K. Katoh, H. Tokisue, and T. Kitahara: *J. Jpn. Inst. Light Met.*, 2005, vol. 55, pp. 259–64.

22. K. Nakata, S. Inoki, Y. Nagano, T. Hashimoto, S. Johgan, and M. Ushio: *J. Jpn. Inst. Light Met*., 2001, vol. 51, pp. 528–33.
23. W. Woo, H. Choo, M.B. Prime, Z. Feng, and B. Clausen: *Acta Mater*., 2008, vol. 56, pp. 1701–11.
24. N. Afrin, D.L. Chen, X. Cao, and M. Jahazi: *Mater. Sci. Eng. A*, 2008, vol. 472, pp. 179–86.
25. P. Heurtier, C. Desrayaud, and F. Montheillet: *Mater. Sci. Forum*, 2002, vol. 1357, pp. 396–402.
26. C. Zener and J.H. Hollomon: *Trans. ASM*, 1945, vol. 33, pp. 955–65.
27. A. Ohmori, S. Torizuka, K. Nagai, N. Koseki, and Y. Kogo: *Mater. Trans*., 2004, vol. 45, pp. 2224–31.
28. K.V. Jata and S.L. Semiatin: *Scripta Mater*., 2000, vol. 43, pp. 743–49.
29. D.C. Hofmann and K.S. Vecchio: *Mater. Sci. Eng. A*, 2005, vol. 402, pp. 234–41.
30. Y.S. Sato, M. Urata, and H. Kokawa: *Metall. Mater. Trans. A*, 2002, vol. 33A, pp. 625–35.
31. Y.S. Sato, M. Urata, H. Kokawa, K. Ikeda, and M. Enomoto: *Scripta Mater*., 2001, vol. 45, pp. 109–14.
32. Y.S. Sato, Y. Kurihara, S.H.C. Park, H. Kokawa, and N. Tsuji: *Scripta Mater*., 2004, vol. 50, pp. 57–60.
33. Y. Takigawa, M. Honda, T. Uesugi, and K. Higashi: *Mater. Trans*., 2008, vol. 49, pp. 1979–82.
34. J. Liao, M. Hotta, K. Kaneko, and K. Kondoh: *Scripta Mater*., 2009, vol. 61, pp. 208–11.
35. M.R. Barnett, Z. Keshavarz, A.G. Beer, and D. Atwell: *Acta Mater*., 2004, vol. 52, pp. 5093–5103.
36. J.A. Esparza, W.C. Davis, E.A. Trillo, and L.E. Murr: *J. Mater. Sci. Lett*., 2002, vol. 21, pp. 917–20.
37. C.I. Chang, C.J. Lee, and J.C. Huang: *Scripta Mater*., 2004, vol. 51, pp. 509–14.
38. R.D. Doherty, D.A. Hughes, F.J. Humphreys, J.J. Jonas, D. Juul Jensen, M.E. Kassner, W.E. King, T.R. McNelley, H.J. McQueen, and A.D. Rollett: *Mater. Sci. Eng. A,* 1997, vol. 238, pp. 219–74.
39. P. Cao, L. Lu, and M.O. Lai: *Mater. Res. Bull*., 2001, vol. 36, pp. 981–88.
40. T.B. Massalski: *Binary Alloy Phase Diagrams*, ASM INTERNATIONAL, 1986, pp. 170–72.
41. J.A. Esparza, W.C. Davis, and L.E. Murr: *J. Mater. Sci*., 2003, vol. 38, pp. 941–52.
42. J.D. Robson and P.B. Prangnell: *Acta Mater*., 2001, vol. 49, pp. 599–613.